PHGN 326 - Advanced Physics Lab II

LAB #1: Basic phenomenology of NaI(Tl) gamma ray detector, MCA, statistics

Brennan Fieck
PH326 Section B Lab Group R-11
Experiment Date: 26th of January, 2017
Report Due Date: 2nd of February, 2017

Abstract

A NaI(Tl) scintillation detector was used in recording γ emissions produced by ^{137}Cs and ^{60}Co. From measurements taken of these sources, efficiencies of the apparatus used in terms of a ratio of incident photons to detected photons were calculated at various photon energies. The apparatus performed with 1.6% efficiency for incident photons with 622 keV of energy, 1.8% efficiency when they had 1173 keV, and 2.0% when they had 1332 keV. Photon counts were also evaluated at various distances, to establish a relationship between distance d from a gamma source and photon density. The trend for a detector of the size and shape used was found to be

$$\text{Number of Photons Detected} = \frac{1257 \pm 120}{d^{1.52 \pm 0.064}} + 0.3 \pm 1.1.$$

Grade	Score	Available
Abstract and Cover Pg.		5
Fig. & Plt.		10
Data & Error Ana.		10
Writing		10
Total		35

1 Introduction

The primary purpose of this lab was merely to familiarize students with the apparatus and data collection and analysis procedures which will be used in future labs. Furthermore, Lab #1 served as a practical introduction to the use of the Maestro®software suite and the `Python-XY` package used for plotting data. As another secondary objective, the lab concerned itself with the emission spectra of ^{137}Cs, ^{60}Co and predictions about the emission characteristics of ^{40}K sources.

2 Apparatus

2.1 Layout

The basic layout of the lab's apparatus didn't change significantly over the course of data collection; a very basic diagram is shown in Figure 1.

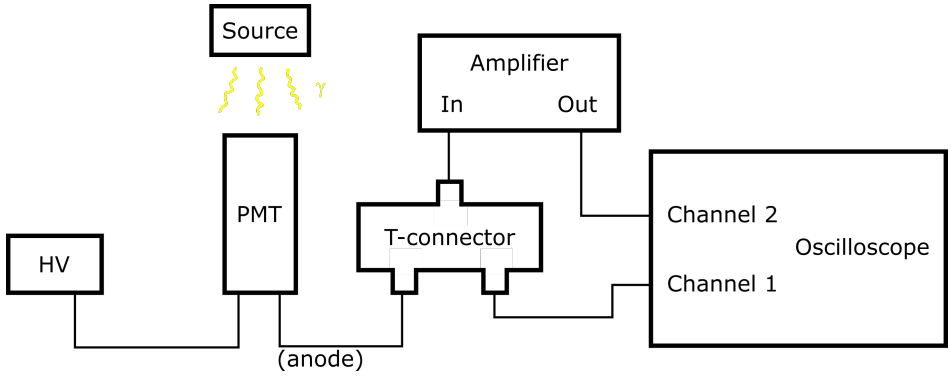

Fig. 1: Basic Illustration of Lab Setup

As shown, the lab utilized a Photomultiplier Tube (PMT) to count incident photons, and generating a signal which was captured both directly and after amplification by the Oscilloscope (or Maestro®software). The PMT requires a high-voltage power source (HV) to function, and output can be measured from the anode or dynode of the PMT; in this particular lab output was measured from the anode as indicated in Figure 1.[1] A notable exception to this layout occurs when the Amplifier's output is connected to the station's computer through a Multi-Channel Analyzer (MCA) for data collection through Maestro®, rather than Channel 2 of the Oscilloscope.

2.2 Sources

The sources used in this lab were as follows:

- ^{137}Cs, 5 μCi, Dated Nov 2015, Half-Life: approx. 30.7 years
- ^{60}Co, 1 μCi, Dated Jan 2015, Half-Life: approx. 5.27 years
- ^{137}Cs, 5 μCi, Dated Dec 2004, Half-Life: approx. 30.7 years

Measurements later in the report will indicate which source was used. It should also be noted that some measurements were taken without any source.

2.3 Photomultiplier Tube

When gamma rays are emitted by a source, before they actually reach a PMT, strictly-speaking they first are picked up by a scintillator. The scintillators used in this lab use NaI(Tl) crystal (Sodium Iodide doped with Thallium) to interact with incident gamma rays. The scintillator operates by taking advantage of the high density of electrons in the crystal which generates favorable conditions for the photoelectric effect and Compton Scattering to take place. At the photon energies encountered in this lab, Compton Scattering is the dominant method of photon absorption.[5] Once photoelectrons are emitted by the scintillator, each representing an incident gamma ray photon, they then

[1] See Section 2.3.

impact a phosphor layer connecting the scintillator to the actual PMT, which itself emits a photon. A cross-section of a PMT showing the basic principles of its operation is shown in Figure 2.

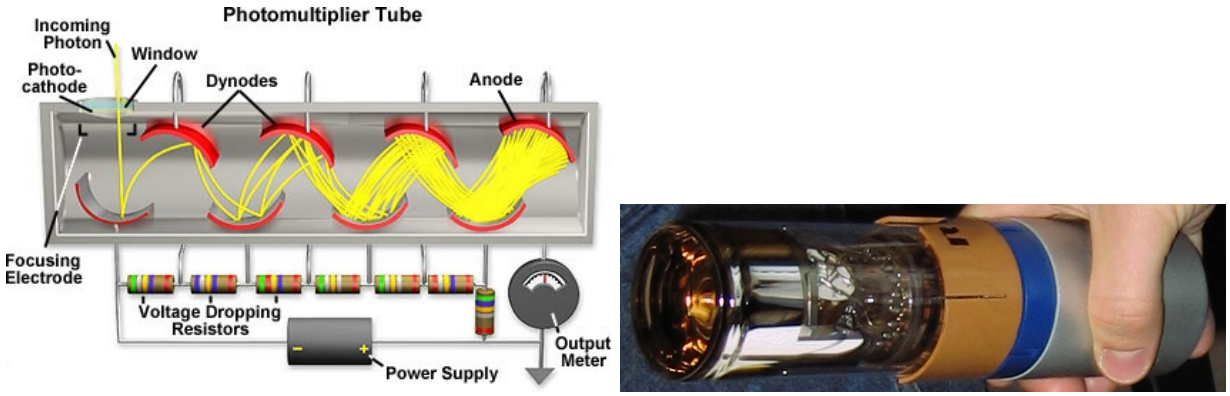

Fig. 2: Photomultiplier tube [2].

This photon is then directed to a photocathode which liberates an electron from said cathode. This electron impacts an electrode with high positive potential, called a "dynode" which in turn liberates more electrons that are attracted to the next, even higher positive potential dynode and so the process continues until enough electrons are generated to induce a voltage pulse on the PMT's output.[4][2] https://preview.overleaf.com/public/qncwprtyhnjq/images/aace367dc0282af263d8f2f2cd8871bcf0afb90d.jpeg A sketch of the system as a whole is shown in Figure 3.

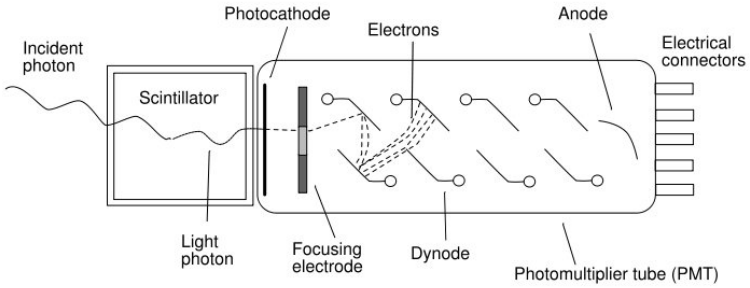

Fig. 3: NaI(Tl) detector, including the crystal, the optical coupling, and the photomultiplier tube.

3 Data Collected

One of the first observations made was of the oscilloscope's output from both the amplified and un-amplified PMT signals for ^{137}Cs. For the source dated November 2015, a sketch of the oscilloscope output and for comparison an image captured from Maestro®are shown in Figure 4.

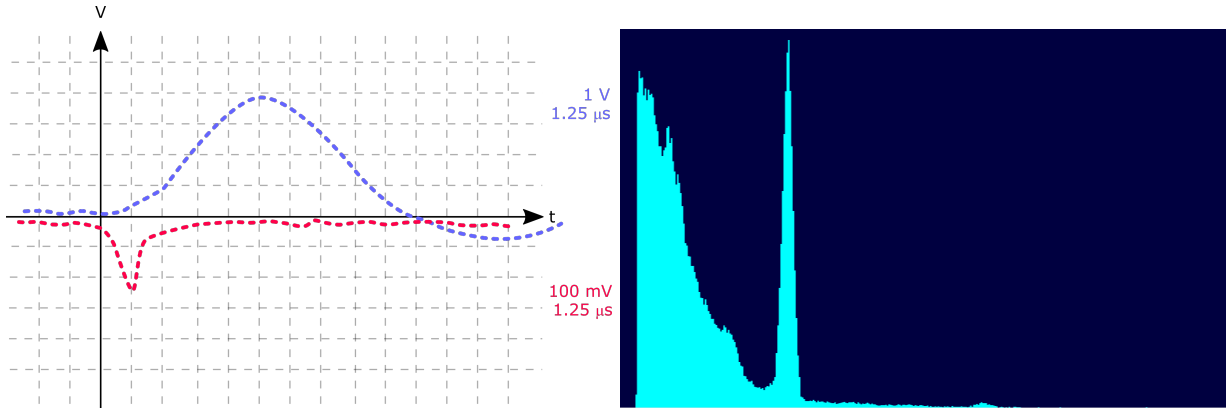

Fig. 4: Left: A Sketch of Oscilloscope Output - Right: Linear Plot of Cesium Emission

Notice that the red signal (Channel 1) is the un-amplified output, while the blue signal (Channel 2) is the amplified signal. Their respective scales are shown to the right of the graph, as set on the oscilloscope.

To help grasp what constitutes a photo-peak, measurements were taken of the number of counts at the photo-peak of the emission from the ^{137}Cs source that was dated November 2015. Ten measurements were made, and the results thereof are shown in Table 1.

Trial	**Counts**
1	988
2	988
3	987
4	976
5	953
6	938
7	962
8	989
9	972
10	973

Tab. 1: Photo-peak Counts ($\mu = 973$ Counts, $\sigma = 17.2$ Counts)

A fundamental part of the lab involved measuring the photo-peaks of the sources specified in section 2.2. Figure 5 shows a qualitative comparison of the spectra collected, on a linear scale.

Fig. 5: Top: ^{137}Cs Emission Data - Bottom: ^{60}Co Emission Data

These spectra were collected over a period of 5 minutes (live time) each, using the ^{137}Cs source dated November 2015 and the only ^{60}Co source, and for both collection periods the HV supply was set to 750 V.
The collected spectra were used to calibrate the Maestro®software as well as to find the "bins"[2] which represented the peak energy emissions of the sources. The calculated peak bins, emission energies, and associated Full Width Half Maximum (FWHM) values are shown in Table 2.

Source	Energy (keV)	Peak (bin)	Fit FWHM (bin)	Peak Counts
^{137}Cs	661.657±0.0003	126±19.15	45.09	5239
^{60}Co	1173.228±0.0003	220±10.48	56.12	438
	1332.492±0.0004	248±10.10	54.05	341

Tab. 2: Spectral information from MAESTRO®. Energy from [8]

As part of the lab, data was collected at varying distances from a ^{137}Cs source for later analysis. The collected data is given in Table 3. Each measurement was taken over a period of 5 seconds (live time), and the measurement was taken from bin 126 (out of 2048 across the entire spectrum), which was the bin calibrated to the ≈662 keV peak of ^{137}Cs's primary mode of gamma emission. The source used for these collections was the one dated December 2004.

Distance (cm)	Counts	Count Rate (Counts/s)
5.0 ± 0.71	549 ± 23.4	110 ± 4.7
10.0 ± 0.707	186 ± 13.6	37.2 ± 2.72
15.0 ± 0.707	109 ± 10.4	21.8 ± 2.08
20.0 ± 0.707	72 ± 8.5	14 ± 1.70
25.0 ± 0.707	53 ± 7.3	11 ± 1.47
30.0 ± 0.707	40 ± 6.3	8.0 ± 1.3
35.0 ± 0.707	36 ± 6.0	7.2 ± 1.2
40.0 ± 0.707	11 ± 3.3	2.2 ± 0.66
45.0 ± 0.707	23 ± 4.8	4.6 ± 0.96
50.0 ± 0.707	15 ± 3.9	3.0 ± 0.78

Tab. 3: Count Rate at Various Distances from ^{137}Cs Source

At one point in the lab, data was also collected over 1 second (live time) intervals for extremely low count rates, which was used in a comparison against Poisson Distributions later. These measurements were taken using the Cesium source dated in December 2004, and are displayed in a simple format in Table 4. The counts were collected

[2] "Bins" here refers to the slots into which counts were placed, each representing 1/2048$^{\text{th}}$ of the measurable spectrum.

in bin 126 (again out of 2048 total), which was calibrated as the ≈662 keV peak gamma emission for the ^{137}Cs source. The HV supply was set to 500V for these measurements.

Number of Counts	Number of Times Measured
0	7
1	24
2	22
3	32
4	10
5	4
6	3

Tab. 4: Low-Count Data Collection

It should be noted that although the instructions stated that 100 measurements were to be taken, this table contains 102 measurements due to an error in keeping track of how many had already been taken.

4 Data Analysis

4.1 Relation Between HV Setting and Photo-peak

Note that in Figure 4, the amplified oscilloscope signal peaks between 3 and 4 Volts. Now notice that the photo-peak shown on the Maestro®graphic occurs at between 1/3$^{\text{rd}}$ and 1/4$^{\text{th}}$ of the total spectrum length. As the HV voltage level is turned up, the peak will shift to the right. This is how the MCA scales voltage levels; higher potentials are assumed to result from higher-energy initial photons. Therefore, as the HV's base voltage increases, the counts are shown at higher energies.

4.2 Detector Efficiency

Recall the data presented in Table 2, as well as the source information presented in Section 2.2. Of particular interest are the counts of each photo-peak, the energy of the radiation, and the activity measures of each source. If the efficiency E of the PMT is given by

$$E = \frac{\gamma_d}{\gamma_i}, \tag{1}$$

where γ_d is the number of photons detected by the apparatus and γ_i is the number of photons incident on the detector, then the information provided by this table and listing are sufficient to find the PMT's efficiency. Let γ_d be the detected count at each photo-peak, with an uncertainty provided by the FWHM measure[7]. To find the number of photons incident on the detector, it can be assumed that for any given decay event a photon is ejected from the source on a random trajectory. Given the distance from the source to the detector d, the radius of the detector's face r and the activity of the source a, it is possible to write an expression for a rate of γ_i based on the "Inverse-Squared Law" of radiation[6]. Because that the time the detector was active is known, all that need be done is consider the number of photons emitted to be the total number emitted during that time. So, over a given period of time t, the approximate number of photons incident on the detector is given by:

$$\gamma_i = \frac{at}{4\pi d^2}\pi r^2,$$

which is to say the total number of emitted photons, distributed across a spherical shell at the distance of the detector, and then integrated along the surface of the detector. Our final equation, then is

$$E = \frac{4d^2\pi\gamma_d}{\pi r^2 at} = \frac{4d^2\gamma_d}{r^2 at} \tag{2}$$

The calculated efficiencies of the PMT for different energies of incident photons is shown in Table 5.

Source	Energy of Photons (keV)	Calculated Efficiency
^{137}Cs	≈622	0.016
^{60}Co	≈1173	0.018
^{60}Co	≈1332	0.020

Tab. 5: PMT Efficiency for Different Photon Energies

The values used (besides activities) were as follows:

- $d = 20.0$ cm
- $r = 3.1$ cm
- $t = 5$ min

The fact that 5 appears to show increasing efficiency as photon energy increases is comforting, even if the actual efficiency calculated is not. This makes sense because higher energy photons are more likely to give electrons enough energy to overcome the work function of their material. Of course, this approach to calculating the efficiency has several over-simplifications and assumptions. First, it assumes that the source radiates perfect distributions in a perfect sphere, which actually isn't too bad considering the sheer number of photons radiated. Then, the assumption is made that the space between the source and the detector is free of any obstruction, when in fact it is packed with air which could absorb or deflect photons. Likewise, the housing of the source was not taken into account, which has a significant impact on how radiation is allowed to spread. Finally, the shape of the detector is not a section of a spherical shell, so the actual calculation of incident radiation should account for the radiation spreading out an extra ≈1.5 cm between when it hits the detector's center and when it hits the edges - though this probably accounts for very small error, considering the large photon density and relatively small increase in surface area caused by this expansion.

4.3 Energy/Bin Relationship

The relation between energy and bin number is extrapolated from the measured bin numbers and given emission energies of the sources. The data is given in Table 2, and shown graphically in Figure 6

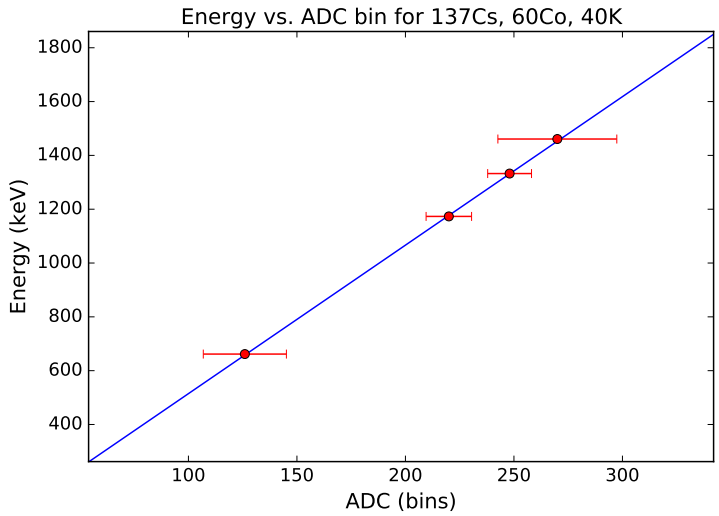

Fig. 6: Energy Related to Bin

The 4^{th} data point in Figure 6 is the estimated location of the ^{40}K photo-peak, which was found by first calibrating Maestro®with the other three data points, then finding what bin ≈ 1332 keV corresponded to. The error was calculated using the FWHM value of the peak that occurred where this energy was encountered, and using the energy error from [8]. The actual numbers are

Emission energy: 1460.822±0.0006 keV, Peak Bin: 270±27.40, FWHM: 64.50.

The linear fit for this graph takes the form:

$$\text{Energy (keV)} = 5.51812934 \pm 0.06020538 \text{ keV/bin number} \times \text{bin number} - 37.20553693 \pm 13.66976587 \text{ keV}. \quad (3)$$

Error due to bin number was calculated using FWHM of the peak of the bin in question[7].

4.4 Count Rates and Distance

Recall Table 3 where data for photo-peak counts was presented with respect to varying distances between detector and source. In Figure 7, this data is shown against fits of the form $A/r^n + B$ when n is 1, 2, or 3. The χ^2 values are given in Table 6.

n	χ^2
1	37.8
2	8.46
3	30.2

Tab. 6: χ^2 Values for Count Rate Fit Curves

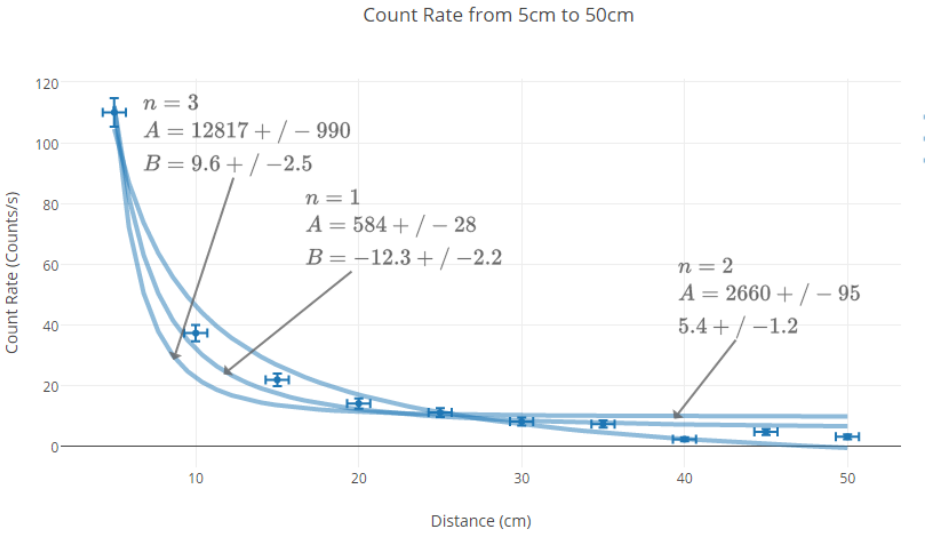

Fig. 7: $n = 1, 2, 3$

The closest fit here appears to be $n = 2$, which is supported by the fact that this curve has the smallest χ^2 value, and a comforting thought as it confirms the "Inverse Squared Law" of radiation[6]. Figure 8 shows a curve where n was kept as a free parameter, and the best fit apparently came from an n value a little bit over 2, which fits the earlier observation with fixed n.

4.4.1 Error

Error bars for Figures 8 and 7 were calculated separately for each axis. The horizontal error bars are the result of the method used to ensure separation distance between the detector and source; a measuring tape with a resolution of up to $1/10^{th}$ of a cm. Furthermore, the fixture in which the source rested had a well on the detector-facing side which was not accounted for during measurement, but was afterwards measured to be ≈3.1 cm deep. Therefore, the error in measured distance is constant for each measurement (before significant figures) at

$$\sigma_{\text{dist}} = \sqrt{\frac{1}{20}^2 + 3.1^2} \approx 0.707.$$

The vertical error bars are a result of the propagation of error from counting the peaks. Timing is handled by the computer, so any error in that ultimately comes down to circuit delay or hardware error. This is negligible in the

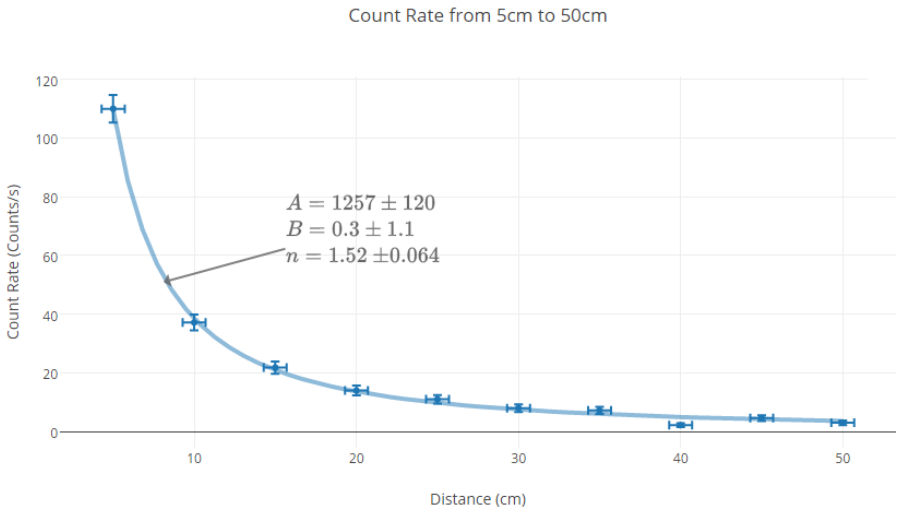

Fig. 8: n as a Free Variable

face of human error and the error induced by MCA resolution. Therefore, to account for error in count rate, $\sqrt{n}$ for n counts was used [7].

$$\sigma_{\text{time}} \approx 0 \rightarrow \sigma_{\text{rate}}^2 = \frac{\delta \text{ rate}}{\delta \text{ counts}}^2 \left(\sqrt{\text{counts}}\right)^2 \rightarrow \sigma_{\text{rate}} = \sqrt{\left(\frac{\sqrt{\text{Counts}}}{\text{time}}\right)^2} = \frac{\sqrt{\text{Counts}}}{\text{time}}$$

where time was kept constant at 5 seconds (live time).

4.5 Low Count Rate Measurements

Recall the data from Table 4. For more effective visualization, this data is reiterated on the left side in Figure 9. On the right side of that same figure is the same data, but overlaid with red dots indicating the shape of a Poisson Distribution with the same mean.

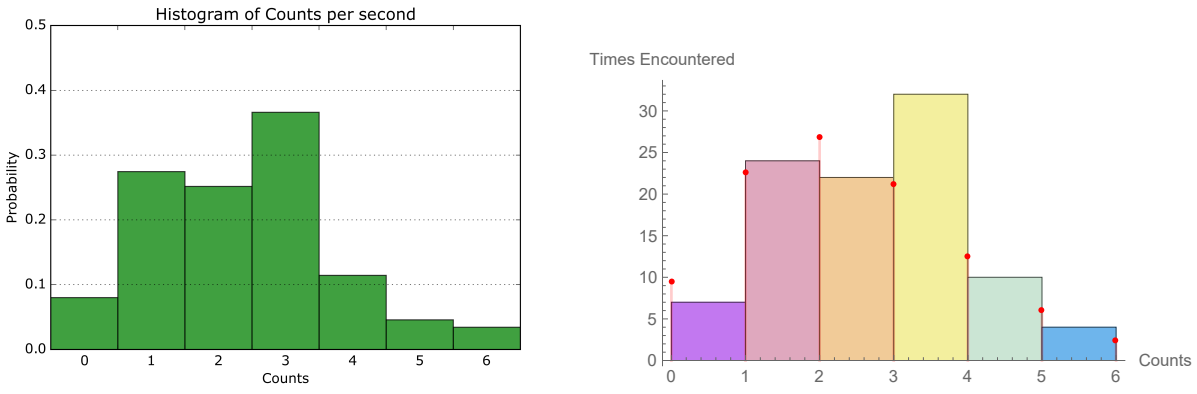

Fig. 9: Left: Low-Count Measurements - Right: Counts Fit With Poisson Distribution ($\mu = 121/51 \approx 2.37$)

Needless to say, this histogram doesn't quite match up with that of an ideal Poisson Distribution. Actually, much of the data looks consistent, but the "3" column is roughly twice the size it ought to be. It's difficult to fathom why this happened; it ought to be independent of scaling, which is to say that even if a few hundred counts per second were allowed that should only shift the distribution's mean. Measurement was handled by the MCA, so time-wise they ought to have been accurate to within a few microseconds at most. The bin measured was well away from any observed peaks in background noise, though again that ought not to affect anything. It is unlikely, also that the

hardware somehow failed in such a specific and minute way.

There are only two explanations that seem to be plausible. The first is that possibly the measured bin happened to correspond to a voltage measurement roughly half that of a tiny peak. Then occasionally photons with twice the energy as those that belong in this bin could potentially glance off of one electron, only imparting half of their energy to it, and then scatter into a second electron. If done in just such a way, this might cause two measurements of about half of the culprit photon's energy. This could mess up the distribution by increasing the probability of measuring several photons than the Poisson model predicts (it is worth noting, after all, that the process described cannot possibly contribute to counts of 0).

Or perhaps, more likely, it was simply bad luck. Neither explanation is really very satisfying, however. More than one hundred data points ought to be sufficient to not break the model so thoroughly; common sense implies a mechanism at work other than luck. On the other hand, the scattering angle for a photon at roughly 1244 keV to deposit half its energy is about 37 degrees, which means that the total angle between the photon's trajectory and that of the electron that took half its energy is a little less than 80 degrees; almost perpendicular. If, then, another electron later received the rest of the photon's energy, it would be traveling nearly perpendicular to the first. So the window for both of those electrons to hit the same thing closes fast. Not to mention that such a precise interaction is almost certainly so low as to be discounted immediately.

5 Conclusion

Upon closer inspection, the initially very worrisome matter of the PMT's extremely low efficiency, capping at just over 2% in the energy range of this lab, is actually quite expected. At first, the fact that the widely-respected Hammamatsu laser and light apparatus company's "PMT Handbook" reports that NaI(Tl) scintillator/PMT apparatuses are among the most commonly used - prized for their "high absorption efficiency"[3] - is troubling. However, further digging into the handbook revealed Figure 10. The figure shows that the effective range for efficient NaI(Tl) scintillators lies roughly between 350 nm and 450 nm[3]. The photon wavelengths encountered in this lab were orders of magnitude outside this range, from about 0.001 nm to about 0.002 nm (from $E = hc/\lambda$). In retrospect, this explains the massive peak at low energy in the Maestro®output. Since PMTs operate most effectively when the method of photon absorption is the photoelectric effect, it seems likely that these low efficiencies indicate dominance of Compton Scattering and interference from significant pair production.

Speaking of signals collected by Maestro®, the seeming linear relationship between energy and bin number implies a relationship between resolution and range of the data it displays. For example, calibrated in the way that it was for the lab (bin #126→622 keV etc.), the software is incapable of displaying energy levels above about 11 GeV, at a resolution of about 5keV/bin (corresponding to the linear fit's slope). Calibrated differently, within a range of 5 keV the software could distinguish variances of as little as about 3 eV, making it highly versatile.

[3] Figure 10 shows *quantum* efficiency, which strictly speaking is not the same as the efficiency calculated in Section 4.2. Rather than a ratio of incident photons to detected photons, the quantum efficiency refers to the ratio of incident photons to subsequently-generated electrons[3]. For practical purposes the difference is primarily that quantum efficiency is only a measure of the scintillator while the calculated efficiency could just as easily be influenced by the PMT.

References

[1] Lawrence Wiencke, Professor for PHGN-326. Instructions for Experiments: Experiment 1: Scintillation Detector. Colorado School of Mines, Physics Department, 2017.

[2] Mortimer Abramowitz & Michael W. Davidson, "Concepts in Digital Imaging Technology, Photomultiplier Tubes", Last modification: Friday, Jul 16, 2004 at 08:16 AM, http://micro.magnet.fsu.edu/primer/digitalimaging/concepts/photomultipliers.html

[3] Hammamatsu, "Photomultiplier Tubes", Third Edition, 2007

[4] Radu Motisan, "NaI Scintillation Probe and Gamma Spectroscopy", Last modification: October 6, 2012, http://www.pocketmagic.net/scintillation-probe-with-photomultiplier-and-nai-crystal/

[5] William R. Leo, "Techniques for Nuclear and Particle Physics Experiments", Springer, 1994, http://link.springer.com/book/10.1007\%2F978-3-642-57920-2

[6] C.R. Nave, "Inverse Square Law, Radiation", Georgia State University, Department of Physics and Astronomy, 2006, http://hyperphysics.phy-astr.gsu.edu/HBASE/forces/isq.html

[7] John R. Taylor, Professor at the University of Colorado Department of Physics."An Introduction to Error Analysis: The Study of Uncertainties in Physical Measurements" Second Edition, 1982.

[8] S.Y.F. Chu, L.P. Ekstrm, and R.B. Firestone1. "The Lund/LBNL Nuclear Data Search", Last Modification:February 1999, http://nucleardata.nuclear.lu.se/nucleardata/toi/perchart.htm

A Supplemental Figures

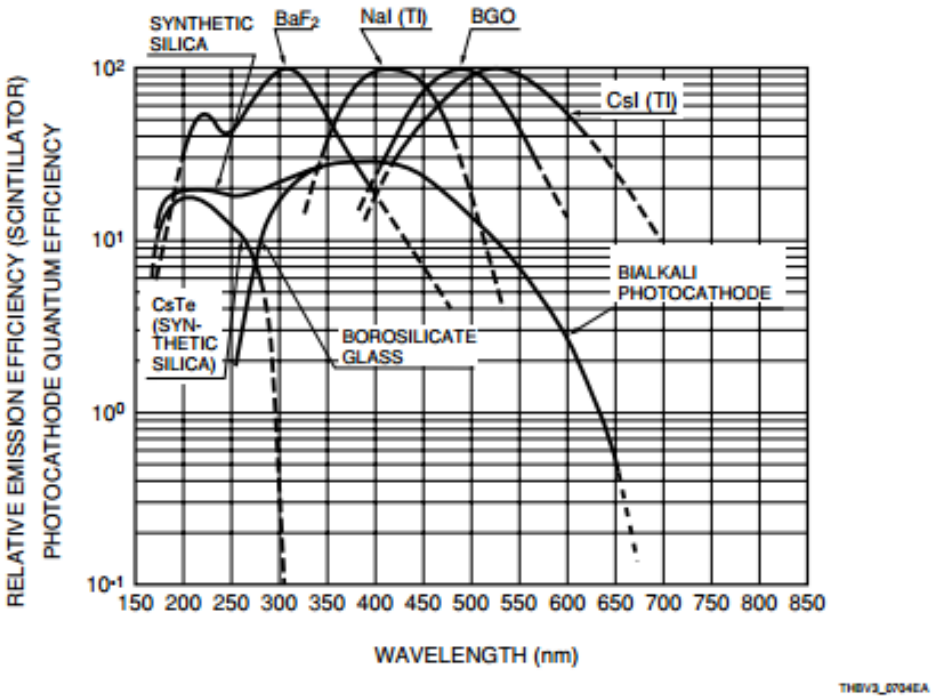

Fig. 10: Efficiencies of Various PMT Apparatuses as Functions of Wavelength

A.1 Maestro®Screen Captures

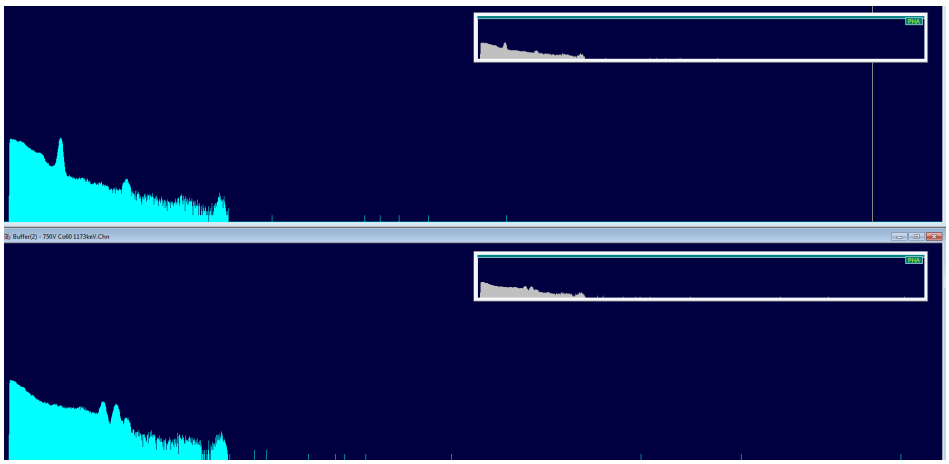

Fig. 11: Top: Log Plot of ^{137}Cs Emission - Bottom: Log Plot of ^{137}Co Emission

Fig. 12: Linear Plot of Cobalt Emission Spectrum

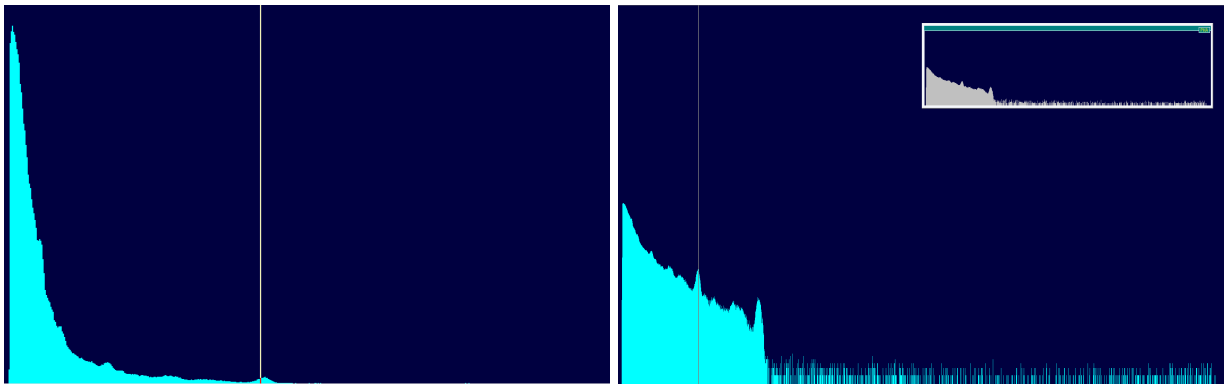

Fig. 13: Left: Linear Plot of MCA Output with no Source - Right: Log Plot of MCA Output with no Source